Supplementary Information for Interfacial atomic orbital controlled spin-hybridization proximity effect in vdW heterostructure

Liyenda Gogoi[1], and Pritam Deb[1*]

[1] *Advanced Functional Materials Laboratory, Department of Physics, Tezpur University (Central University), Tezpur-784028, India.*

(Dated: October 27, 2025)

* Corresponding Author: pdeb@tezu.ernet.in (Pritam Deb).

Different heterostructures depending on stacking

Depending on the position of C and Sn atom relative to Cr, S and Te, five different heterostructures are considered for both CrSTe/SnC and CrTeS/SnC having Te and S on interface respectively. These structures are shown in figure S1. Heterostructures are named based on the relative position of Sn and C on top or hollow position of the interfacial layer of CrSTe. Figure S1(a) shows the heterostructure of SnC with CrSTe having SnC on the Te side of CrSTe. From the top view and side, it can be seen that, C atom is aligned with the Cr atom. It is represented by Cr-C in the name of the heterostructure. Further, C atom lies on the hollow region abpve the interfacial atomic layer of CrSTe consisting of Te atom, therefore the naming is extended to Cr-C(h). Again, since Sn atom is aligned with the S atom and lies on the hollow position above the interfacial layer Te, therefore this is represented by S-Sn(h). Hence the name of the heterostructure become Cr-C(h)-S-Sn(h). Here h and t in the nomenclature of the heterostructure represents hollow and top position. Same method is used for naming the other heterostructures. (b) Cr-Sn(h)-S-C(h): C align with S and Cr align with Sn; C and Sn lies on the hollow position above Te. (c) Cr-Sn(h)-Te-C(t): C align with Te and Sn align with Cr; C and Sn lies on the top and hollow position respectively above Te. (d) Te-C(t)-S-Sn(h): C align with Te and Sn align with S; C and Sn lies on the top and hollow position respectively above Te. (e) Te-Sn(h)-S-C(t): C align with S and Sn align with Te; C and Sn lies on the top and hollow position above Te respectively. CrTeS/SnC heterostructure - (f) Cr-C(h)-S-Sn(t): C align with Cr and Sn align with S; C and Sn lies on the hollow and top position above S respectively. (g) Cr-Sn(h)-S-C(t): C align with S and Sn align with Cr; C and Sn lies on the top and hollow position above S respectively. (h) Te-Sn(h)-S-C(t): C align with S and Sn align with Te; C and Sn lies on the top and hollow position above S respectively. (i) Te-C(h)-Cr-Sn(h): C align with Te and Sn align with Cr; C and Sn lies on the hollow position above S. (j) Te-C(h)-S-Sn(t): C align with Te and Sn align with S; C and Sn lies on the hollow and top position above S respectively.

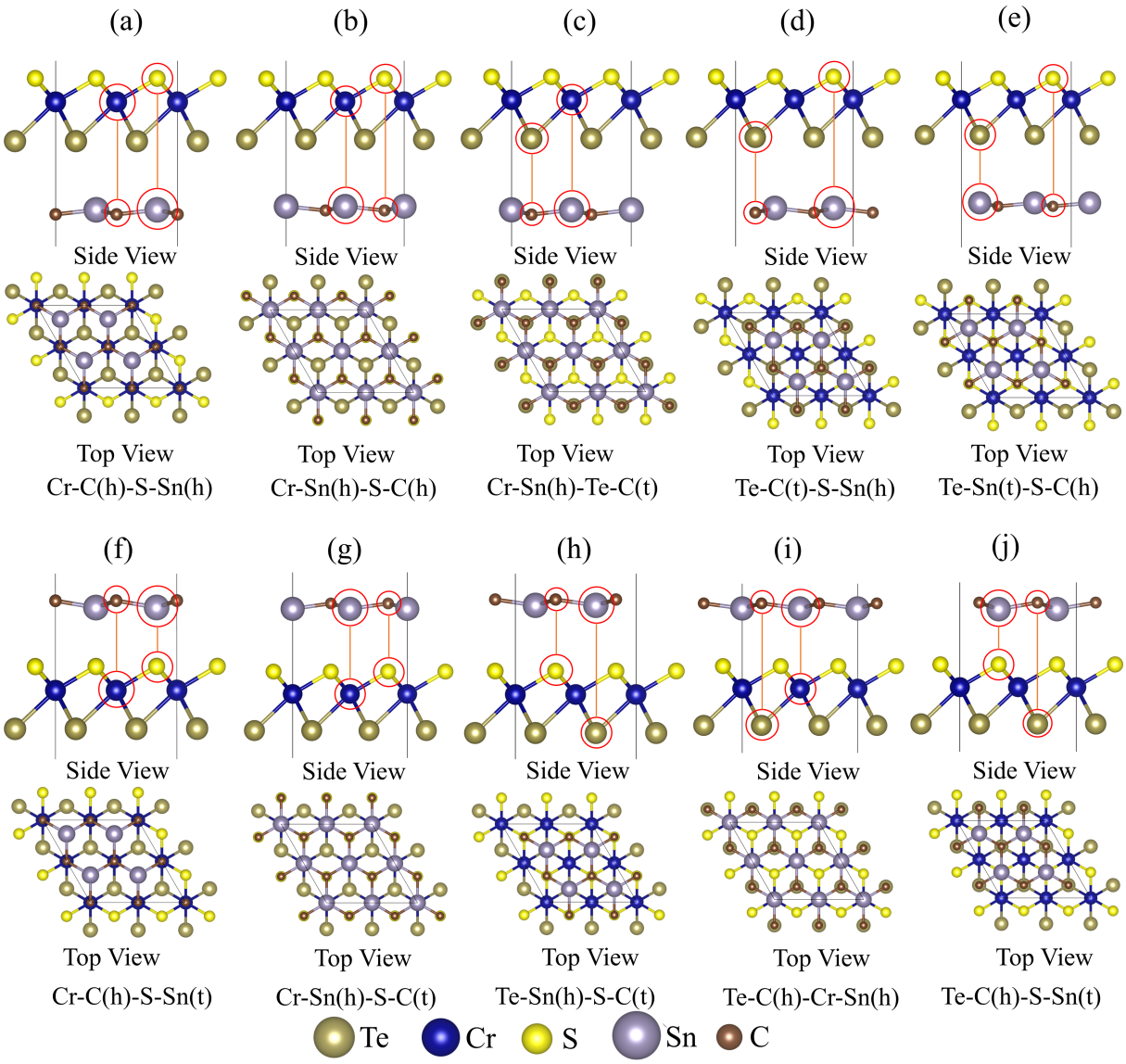

Fig. S1. Side and top view of stacking dependent heterostructures. CrSTe/SnC heterostructure - (a) Cr-C(h)-S-Sn(h): C align with Cr and Sn align with S; C-hollow, Sn-hollow. (b) Cr-Sn(h)-S-C(h): C align with S and Cr align with Sn; C-hollow, Sn-hollow. (c) Cr-Sn(h)-Te-C(t): C align with Te and Sn align with Cr; C-top, Sn-hollow. (d) Te-C(t)-S-Sn(h): C align with Te and Sn align with S; C-top, Sn-hollow. (e) Te-Sn(h)-S-C(t): C align with S and Sn align with Te; C-top, Sn-hollow. CrTeS/SnC heterostructure - (f) Cr-C(h)-S-Sn(t): C align with Cr and Sn align with S; C-hollow, Sn-top. (g) Cr-Sn(h)-S-C(t): C align with S and Sn align with Cr; C-top, Sn-hollow. (h) Te-Sn(h)-S-C(t): C align with S and Sn align with Te; C-top, Sn-hollow. (i) Te-C(h)-Cr-Sn(h): C align with Te and Sn align with Cr; C-hollow, Sn-hollow. (j) Te-C(h)-S-Sn(t): C align with Te and Sn align with S; C-hollow, Sn-top.

Different parameters for different heterostructures are tabulated in Table S1. The listed the relative energies per unit cell (E_r) of the heterostructures with respect to the most stable heterostructure, interlayer separation (d), formation energy (E_f) and binding energy (E_b). (E_r) is calculated by subtracting the energy of the most stable heterostructure from the corresponding heterostructures. From the table it is found that the Te-C(h)-S-Sn(t) with interlayer separation 2.84 Åis the most stable configuration for CrTeS/SnC heterostructure and Cr-C(h)-S-Sn(h) with interlayer separation 3.37 Åis the most stable configuration for CrSTe/SnC heterostructure. These two structure has the highest value of negative formation and binding energy, which confirms the stability of these two structure over the other stacking structures. The formula for calculation of formation energy and binding energy is presented in the main text.

TABLE S1. Relative energies per unit cell E_r of the heterostructures with respect to the most stable heterostructure, interlayer separation (d), formation energy (E_f) and binding energy (E_b).

Systems	d (Å)	E_r(meV)	E_f (meV)	E_b (meV)
CrTeS/SnC				
Te-Sn(h)-S-C(t)	3.26	145.58	-123.93	-269.11
Te-C(h)-S-Sn(t)	2.84	0	-269.41	-414.60
Te-C(h)-Cr-Sn(h)	2.99	42.17	-227.24	-372.43
Cr-C(h)-S-Sn(t)	2.90	34.94	-234.47	-379.65
Cr-Sn(h)-S-C(t)	3.27	149.2	-120.20	-265.39
CrSTe/SnC				
Te-Sn(t)-S-C(h)	3.69	83.98	-138.97	-260.59
Te-C(t)-S-Sn(h)	3.60	95.63	-127.32	-248.94
Cr-Sn(h)-Te-C(t)	3.57	84.81	-138.84	-259.75
Cr-C(h)-S-Sn(h)	3.37	0	-222.95	-344.57
Cr-Sn(h)-S-C(h)	3.39	14.24	-208.71	-330.32

Curie Temperature

The Curie temperature of the substrate ferromagnet in the heterostructure is calculated using Monte Carlo simulations implemented in VAMPIRE atomistic simulation package[1]. The exchange constants used for the calculation of curie temperature is obtained from the well established four state method[2]. From the calculation the Curie temperature of the system is estimated to be 285 K, which is in same range as other Janus materials [3,4]. The M-T curve is shown in the figure S2.

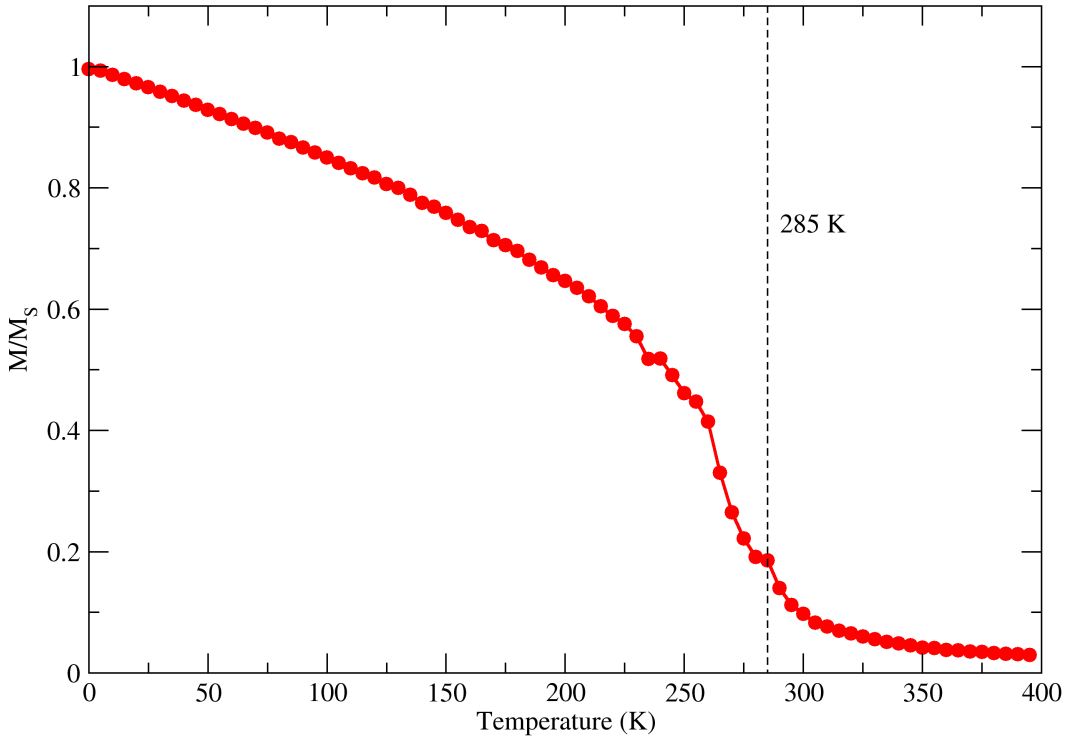

Fig. S2. M-T curve of the substrate ferromagnet in the heterostructure. Curie Temperature is estimated to be 285 K.

Variation of induced magnetic moment with interlayer separation

To check the variation of induced magnetic moment in SnC with interlayer separation, we have considered two heterostructure in addition to the optimized heterostructures. The optimized interlayer separation for CrSTe/SnC and CrTeS/SnC heterostructures are 3.37Å and 2.84Å respectively as shown in the figure S3(a,b). In the optimized CrSTe/SnC and CrTeS/SnC heterostructures, the induced magnetic moments are 0.00 and -0.1225 μ_B respectively. The interlayer separation for the additional two heterostructures are 2.84Å and 3.37Å respectively as shown in figure S3(c,d). In this case, the induced magnetism in SnC layer is 0.00 and -0.06 μ_B respectively. These results confirms that the asymmetry in the magnetic effect of CrSTe on SnC is not governed by the interlayer separation.

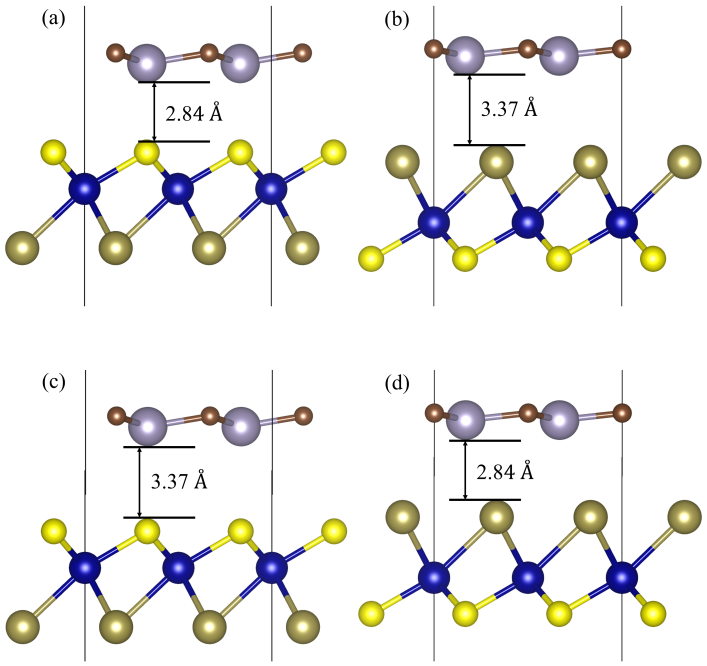

Fig. S3. Heterostructures, considered for the study of the effect of interlayer separation on the induce magnetism. Optimized (a) CrTeS/SnC and (b) CrSTe/SnC. Additional heterostructures (c) CrTeS/SnC with 2.84Å and (d) CrSTe/SnC with 3.37Å

Projected bands structure of SnC in CrTeS/SnC and CrSTe/SnC heterostructure

The atomic resolved band structure of SnC in CrTeS/SnC and CrSTe heterostructure is shown in the figureS4. It compares the atomic resolved band structure of the heterostructures obtained using DFT-D2 and DFT-D3 vdW correction. From the figure, it is evident that, both the correction method give the same band structure. The Figure S4(a,b) shows that the spin splitting around the K-high symmetry point in the CrTeS/SnC heterostructure is contributed by the SnC layer and the value of the spin splitting is 447 meV. It also confirms that there is no spin splitting in SnC in the CrSTe/SnC heterostructure. Further, the absence of contribution of CrSTe to these band around the Fermi level at the K-high symmetry point is presented in the Figure 3 of main text.

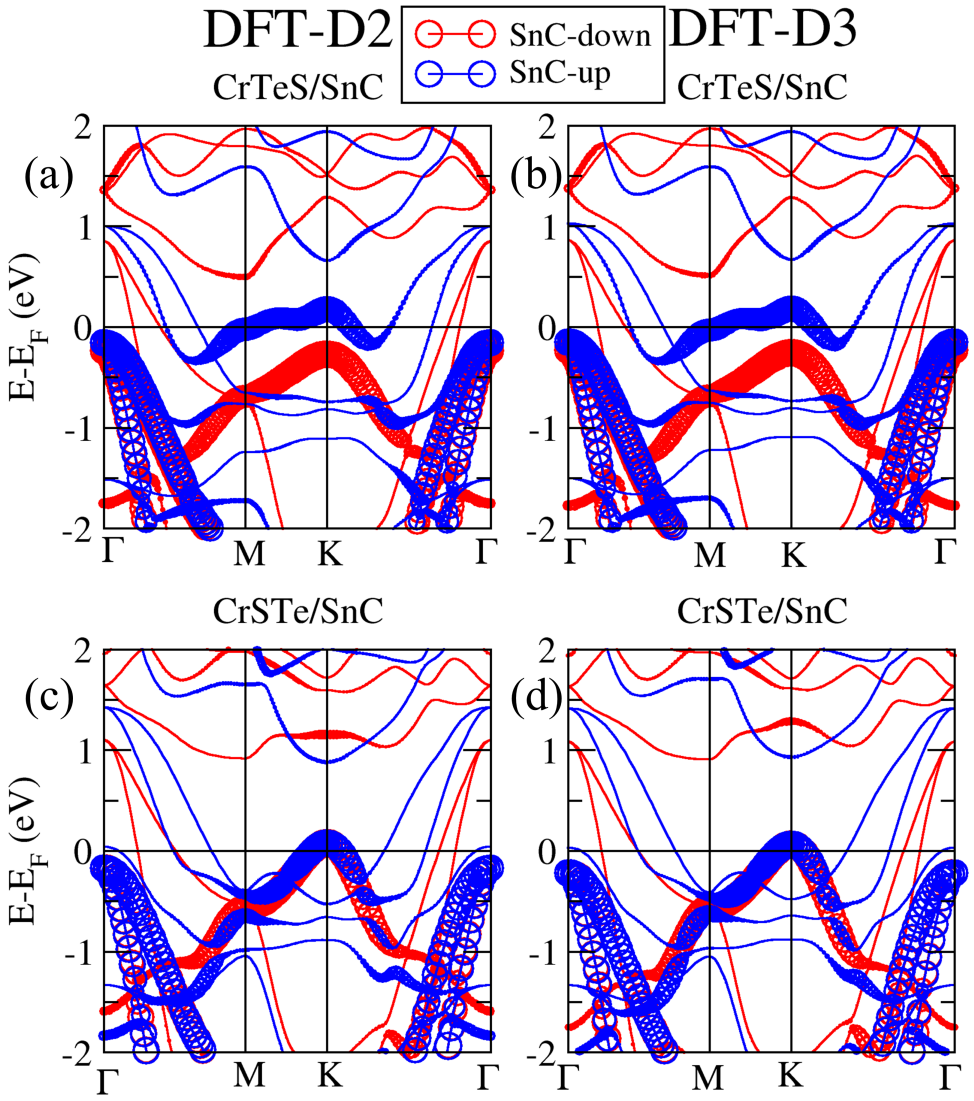

Fig. S4. Atomic resolved band structure of SnC in CrSTe/SnC and CrTeS/SnC heterostructure. (a,b) Contribution of SnC to the band structure of CrTeS/SnC calculated using DFT-D2 and DFT-D3 vdW correction. (c,d) Contribution of SnC to the band structure of CrSTe/SnC calculated using DFT-D2 and DFT-D3 vdW correction. Larger the band higher is the contribution of SnC to the band structure. Only the band line without any circle signifies the absence of contribution of SnC to those particular bands.

Projected Density of states of SnC and CrSTe in CrTeS/SnC heterostructure

The spin polarized PDOS for SnC and CrSTe in CrTeS/SnC heterostructure is shown in the figureS5. From the figure, it is evident that, SnC is metallic for spin up bands whereas SnC has a band gap of 0.73 eV for spin down bands in the CrTeS/SnC heterostructure. This demonstrate the half-metallic character of SnC in the CrTeS/SnC heterostructure.

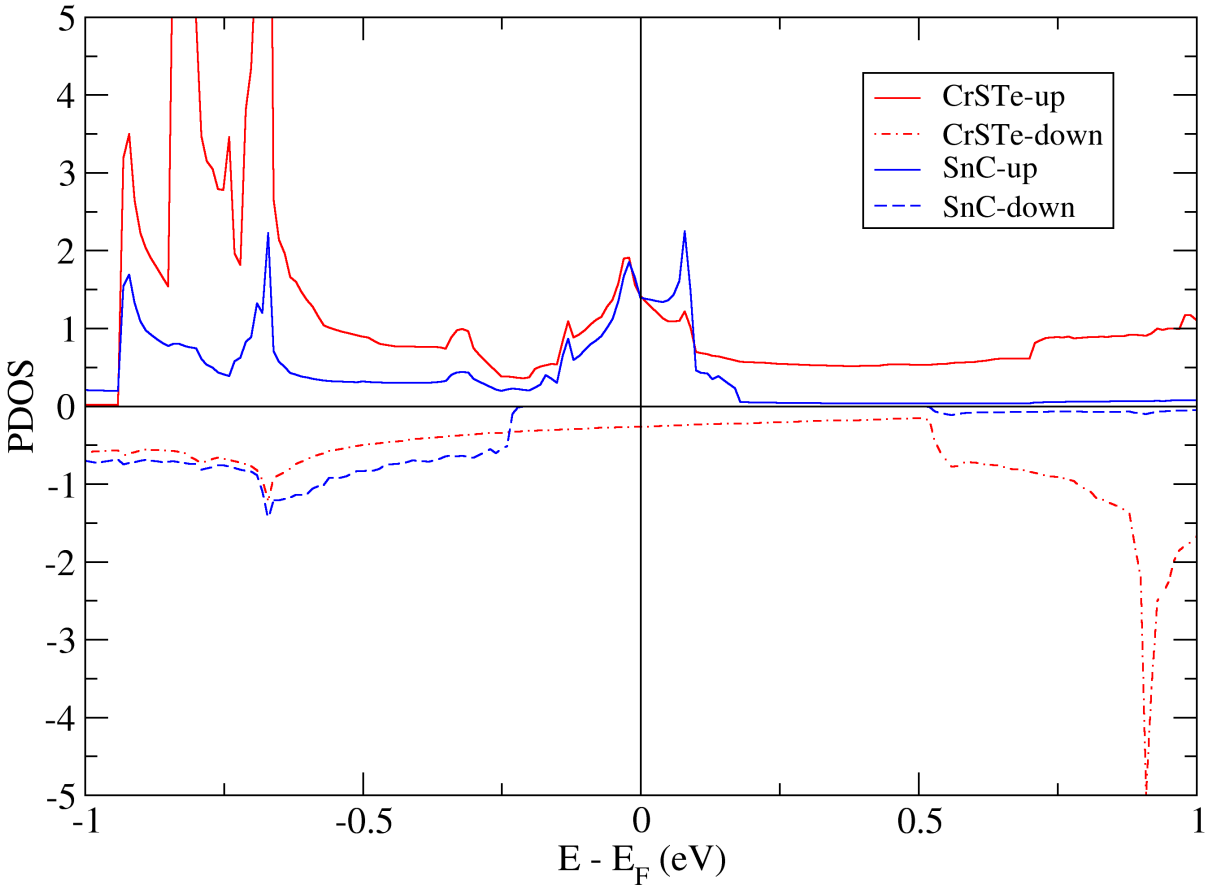

Fig. S5. PDOS of SnC and CrSTe in CrTeS/SnC heterostructure.

Orbital resolved projected band structure of surface atoms of CrSTe

The orbital resolved projected band structures for S and Te are shown in the figure SS6. From the figure it is evident that, the only p_z-up orbitals of S has contributed to the electronic bands at the Fermi level. Other p_z orbitals of S and Te do not contributed to the electronic band at the Fermi level. Hence, hybridization takes place between only p_z-up orbitals of S and SnC.

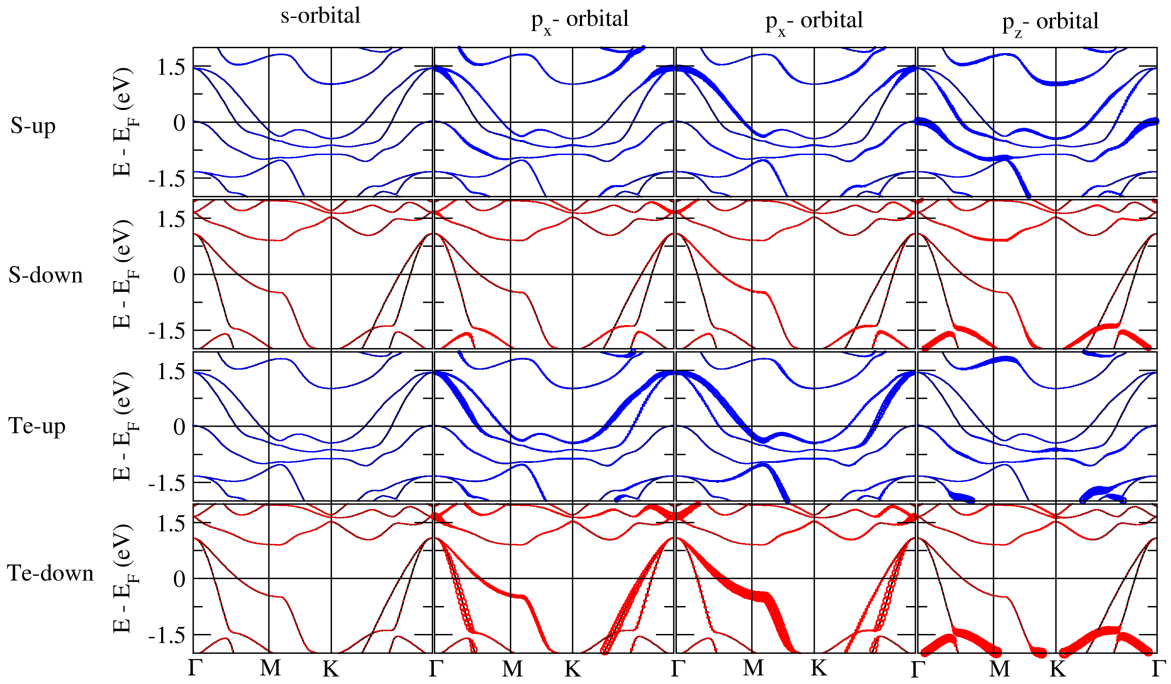

Fig. S6. Orbital resolved projected band structure of CrSTe monolayer. The four panels in the first row represent the projected bands for S-s-up, S-p_x-up, S-p_y-up and S-p_z-up orbital respectively. The four panels in the second row represent the projected bands for S-s-down, S-p_x-down, S-p_y-down and S-p_z-down orbital respectively. Similarly, the third and fourth row represent the projected bands for Te atom.

Orbital resolved projected band structure of C atom in SnC

The orbital resolved projected band structure for C is shown in the figure S7. From the figure it is evident that, the only p_z orbital of C has contributed to the valence band maxima (VBM) of the electronic bands of SnC. Therefore, when heterostructure is formed, the VBM of SnC align with the Fermi level of electronic band structure of CrSTe and at the Fermi level, C p_z orbitals hybridize with the p_z orbitals of the interfacial atoms in the corresponding interface.

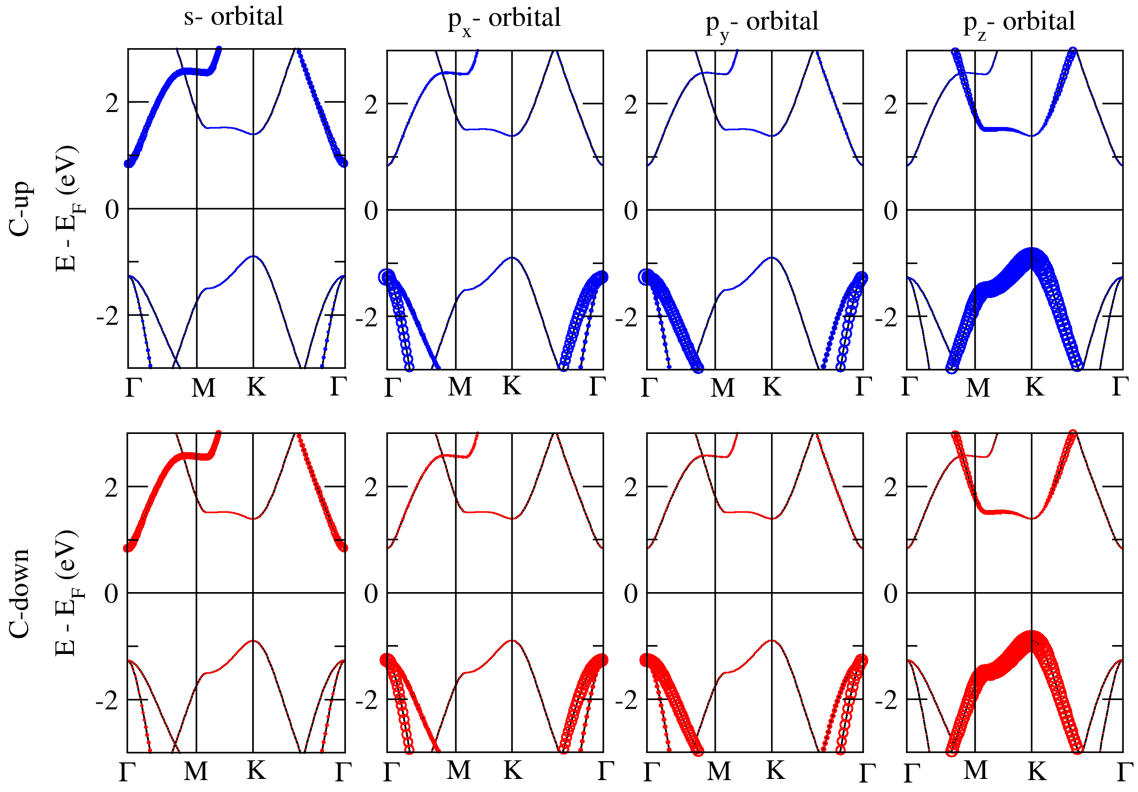

Fig. S7. Orbital resolved projected band structure of C atoms of SnC monolayer. The four panels in the first row represent the projected bands for C-s-up, C-p_x-up, C-p_y-up and C-p_z-up orbital respectively. The four panels in the second row represent the projected bands for C-s-down, C-p_x-down, C-p_y-down and C-p_z-down orbital respectively.

Absence of hybridization and magnetism in Sn

The orbital resolved projected band structure for Sn is shown in the figure S8. From the figure it is evident that, the p_z orbital of Sn has no contribution to the valence band maxima (VBM) of the electronic bands of SnC. When the heterostructure is formed, the VBM of SnC align with the Fermi level of electronic band structure of CrSTe at the Fermi level. But due to the absence of Sn p_z orbitals at the VBM, the orbitals of Sn do not participate in intefacial hybridization and hence no magnetism is induced in the Sn atom of SnC layer in any heterostructures.

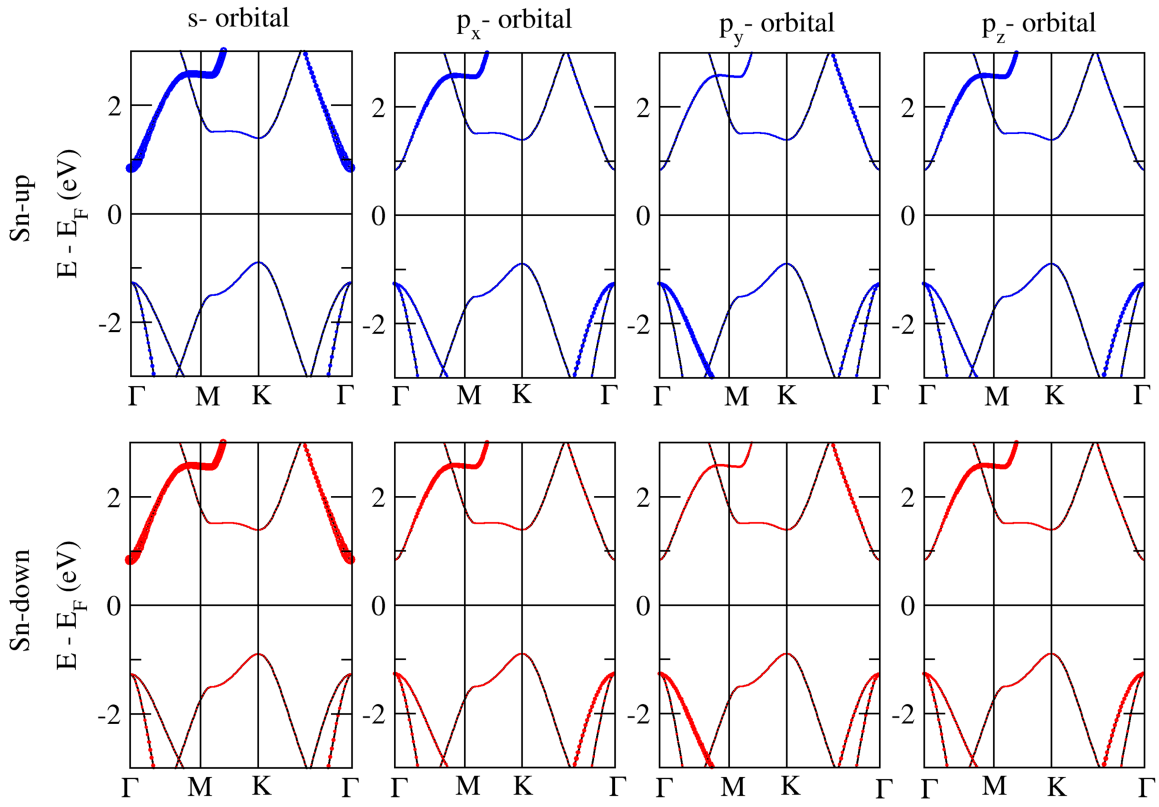

Fig. S8. Orbital resolved projected band structure of Sn atoms of SnC monolayer. The four panels in the first row represent the projected bands for Sn-s-up, Sn-p_x-up, Sn-p_y-up and Sn-p_z-up orbital respectively. The four panels in the second row represent the projected bands for Sn-s-down, Sn-p_x-down, Sn-p_y-down and Sn-p_z-down orbital respectively.

Application of Strain

Compressive and tensile strain is applied in the system by changing the in-plane lattice constant. If a_0 is the in-plane lattice constant of the heterostructure and a is the in-plane lattice constant of the strained system, then strain is given by $(a - a_0)/a_0 \times 100\%$. The variation in the magnitude of induced magnetic moment is shown in the figure S9. From the figure, it is evident that the induced magnetic moment change with change in strain. These changes in strain follow similar trend with the change in contribution of p_z-orbitals from the interfacial atoms.

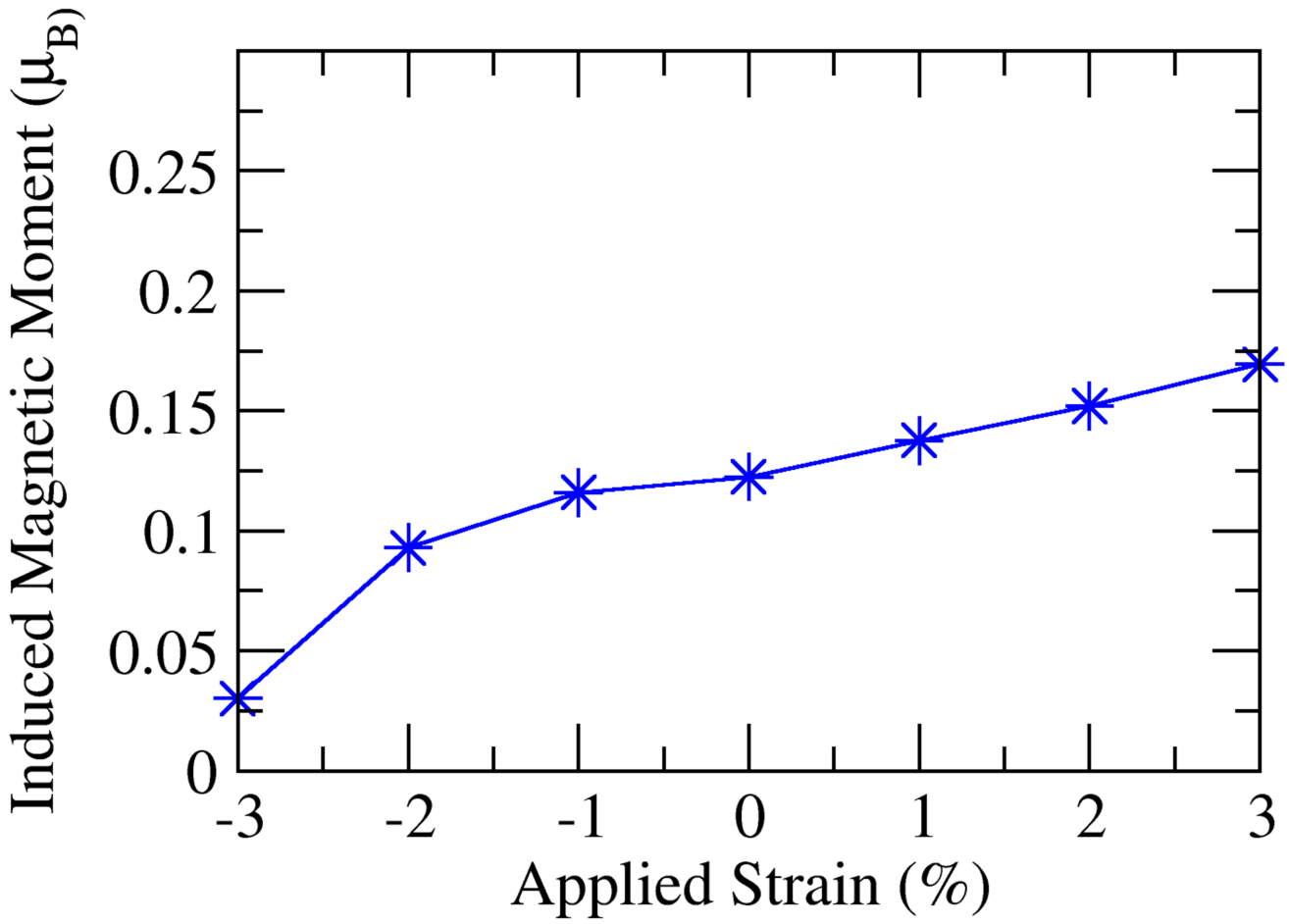

Fig. S9. Variation of induced magnetic moment in SnC with applied strain

References

1. Evans, Richard FL, et al. "Atomistic spin model simulations of magnetic nanomaterials." Journal of Physics: Condensed Matter 26.10 (2014): 103202.

2. Xiang, Hongjun, et al. "Magnetic properties and energy-mapping analysis." Dalton Transactions 42.4 (2013): 823-853.

3. Wu, Yaxuan, et al. "High temperature ferromagnetic metal: a Janus CrSSe monolayer." Physical Chemistry Chemical Physics 25.14 (2023): 9958-9964.
4. Li, Cunquan, and Yukai An. "Two-dimensional intrinsic ferrovalley Janus 2H-VSeS monolayer with high Curie temperature and robust valley polarization." Physical Review Materials 6.9 (2022): 094012.